Interpreting force response patterns of a mechanically driven crystallographic phase transition

Arijit Maitra [*] and Bipin Singh [†]
Department of Applied Sciences, School of Engineering and Technology, BML Munjal University, NH 8, 67 KM Milestone, Gurugram, Haryana 122413, India

(Received 7 October 2021; accepted 5 April 2022; published 20 April 2022)

Mechanically induced crystallographic phase transformation that reflects dynamic stress responses of intrinsically stochastic nature is a pertinent yet much less well understood phenomenon. We focus on understanding the physical significance of stochasticity and how it can enable an inference of principles underlying a crystallographic phase transformation. For interpreting the mechanical responses, a statistical approach of mapping the transformation dynamics to a probabilistic escape of crystallographic states defined on a free-energy landscape is shown to reliably explain the patterns of response. We demonstrate that stochastic responses associated with a structural phase transformation can offer a reliable quantitative tool for unraveling the free-energy profile, intrinsic kinetics, and microscopic details of solid-to-solid crystallographic transitions.

DOI: 10.1103/PhysRevMaterials.6.043404

I. INTRODUCTION

Advances in nanomechanical instrumentation and MEMS (microelectromechanical system)-based devices are offering new approaches in the field of evaluation and characterization of materials [1,2]. Use of these techniques enables precise measurements of how a material responds to an externally imposed displacement or force ramp captured in the form of deformation response-stimulus patterns, e.g., force–displacement or stress–strain correlations. Nano- and micromechanical testing of small submicrometer-sized *single-crystalline* solids have often revealed that the nature of force response patterns is *stochastic* [3,4]. The observed stochasticity has a microscopic basis and arises because of intrinsic fluctuations in the generative mechanisms and evolution of a small number of imperfections in the crystal lattice such as twins, stacking faults, and dislocations [5]. We turn to crystalline metallic systems, where nanoscale stochastic force response patterns offer a powerful yet untapped quantitative perspective of the microscopic mechanisms underlying deformation, which are otherwise inaccessible in classical (bulk) testing methods. An important task of quantitative analyses in dynamic force spectroscopy of materials, discussed here, is to infer the hidden—microscopic—information of deformation rate processes that underlie system level—macroscopic—behavior.

By the term *stochastic* we refer to a nondeterministic nature that is characterizable through a statistical distribution of response variables observed in experiments or simulations, e.g., critical field (force) or time of an observed lattice instability. To allow the significance of stochasticity interpreted, we describe a statistical-mechanical approach for modeling the distribution that ultimately provides insights into a relevant deformation mechanism. We illustrate the model to learn the characteristics of a *twin* mechanism operating underneath the *pseudoelastic* mechanical behavior of a single crystalline titanium nickel alloy [6–8].

In our illustration, the stochasticity manifested in the ensemble of mechanical responses is due to a strain-induced crystallographic *twinning*—a microscopic mechanism—implicated in the isothermal solid-to-solid *martensitic* transformation of an austenite phase to martensite, which in essence involves a change of crystal structure from a body-centered cubic to a predominantly monoclinic system. The stochastic response stems from random and thermally activated microscopic processes, as the austenite lattice restructures into a twinned lattice of the martensite. Apart from fundamental interests, understanding stochastic phase transformation-mediated constitutive responses is important for applications and end-use functionalization of materials. For instance, response fluctuations will have an impact on the accuracy and reliability of tiny actuators and micromachines that are composed of pseudoelastic and shape memory alloys, a class the titanium nickel alloy belongs [9,10].

Solving the inference problem, i.e., what mechanistic properties underlie the stochasticity of transformation-mediated mechanical responses, will have a broader impact on the analyses of nanomechanical testing data. This, however, is yet to be explored in metallic materials. Theoretical and computational models invoking martensitic transformation and microstructural aspects for the treatment of mechanical behavior can be found in a few insightful studies [8,11–14]. Here we show how the intrinsic kinetic properties, free-energy landscape, and the range of microscopic interactions can be reliably inferred for a deformation mechanism associated with an observed distribution of critical forces.

Interpretation of stochastic force responses is based on threefold steps: First, a distribution of a feature variable which is to be modeled, e.g., the *time* of a force response curve to flip abruptly or the *critical force* to generate a lattice twin is required; refer to Fig. 1 (top left). In our simulated responses,

[*] arijit.maitra@bmu.edu.in
[†] Current Address: School of Engineering and Applied Sciences, Bennett University, Greater Noida, Uttar Pradesh 201310, India.

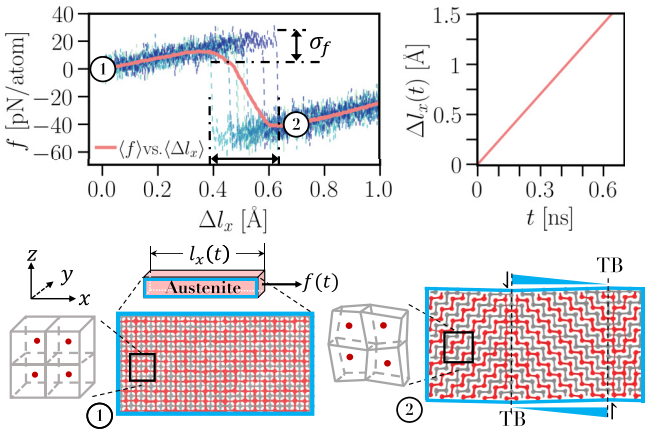

FIG. 1. Stochastic nature of phase transition response. Top left (dashed lines): Uniaxial tensile force, f, vs displacement, Δl_x, of titanium nickel alloy obtained from independent MD simulations performed under identical conditions; rate of extension $\dot{l}_x = 0.00235$ Å/ps, and temperature T = 300 K. Representative atomic views of titanium nickel alloy structure marked ①and ②are shown in the bottom panels. Top right: Imposed tensile extension, Δl_x, vs t, which produced responses of the top-left panel. Bottom left: Schematic deformation of austenite along [100] coinciding with the x axis of the simulation box. A snapshot of the xz cross-section of the simulation box, unstressed at $t = 0$, and four unit cells, B2, is shown. Red and gray dots are titanium and nickel atoms. Bottom right: Atomic arrangement and four unit cells of martensite at $t = 0.32$ ns extracted from a simulation trajectory after relaxation of the peak force. Twin boundaries are labeled TB.

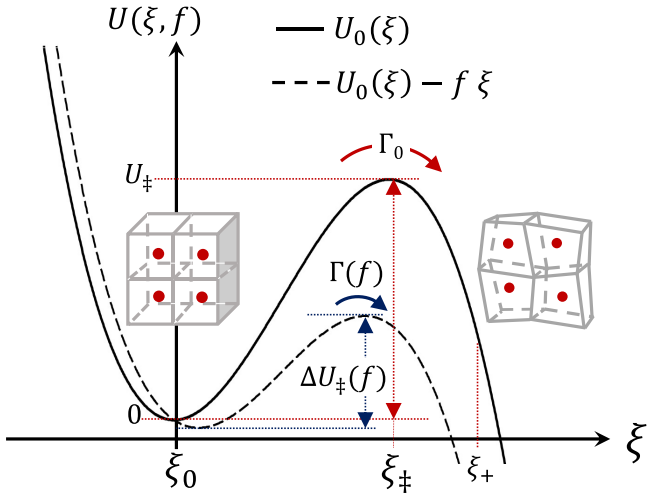

FIG. 2. Free Energy Profile of a Phase Transition. (Solid line) No applied force, $f = 0$; and (dashed line) under applied force, $f > 0$. Austenite phase is associated with a range of the order parameter $\xi \in (-\infty, \xi_\ddagger]$ and martensite to $\xi \in (\xi_\ddagger, +\infty)$ [20].

such recognizable features correlate with the inception of a defect (e.g., twin) mechanism within an initially defect-free (parent austenite) lattice. Second, a model of free-energy landscape that represents the crystallographic states of the defect-free (e.g., parent austenite) and defect (e.g., twinned martensite) lattice identifiable from an order parameter is considered; refer to Fig. 2. Third, a framework for capturing the crystallographic transformation in terms of a probabilistic evolution equation of the defect configuration on the free-energy landscape, perturbed by a known time-dependent stimulus, e.g., strain or stress, is required. We show that the mapping of phase-transformation dynamics as a *random-escape* process over the free-energy barrier, prescribed within a framework of statistical mechanics such as Smoluchowski's equation, can consistently explain the statistical distribution of critical force observed under different strain rates [15–18]. Solving this framework is particularly useful as it provides expressions of perturbation-dependent Kramers [19] escape rates of the parent state over the free-energy barrier, yielding the rate of phase transition as a function of the biasing force. In addition, expressions of probability fluxes and extant probability can be derived, enabling quantitative analyses of the dynamic force response patterns.

In the following sections, the general approach of representing a critical force distribution and a specific model derived using it is described. The utility of the model is demonstrated, and key implications are discussed toward gaining a microscopic perspective of the martensitic structural phase transformation from an analysis of mechanically induced force responses.

II. RESULTS AND DISCUSSION

A. Statistical nature of mechanically induced structural transitions

Transformation of austenite to martensite, in response to a steadily increasing uniaxial tensile strain, is analyzed in a single crystal of titanium nickel alloy from *all-atom* nonequilibrium molecular dynamics simulations (MD) [21]. Strain is applied *quasistatically* and homogeneously to a model specimen in the austenite phase, which has a B2 structure [22] along the [100] direction according to the protocol $\Delta l_x(t) = \dot{l}_x t$, where $\Delta l_x(t) = l_x(t) - l_x(0)$ denotes an instantaneous expansion of the box length l_x in the x dimension, and $\dot{l}_x$ is a constant rate of expansion or displacement applied; refer to Fig. 1. Maximum strain, $[\Delta l_x(t)/l_x(t = 0)]$, applied is restricted to 2.5%. This regime is characterized by twin-mediated pseudoelastic behavior. Note that dislocation slip-based plasticity does not occur in the regime simulated. With progressively increasing strain, a net resistive force $f(t)$ counteracting the deformation, determined from the element, σ_{xx}, of the internal stress tensor is found to develop in the B2 structure (see details in Methods). The mean constitutive response $\langle f(t)\rangle$ vs $\langle \Delta l_x(t)\rangle$ representative of a *macroscopic* behavior is shown where $\langle \cdots \rangle$ refers to an ensemble-averaged value computed as a mean at a given t over all the traces and under identical conditions. The decline of average force beyond the linear elastic regime of austenite correlates with the progress of martensitic transformation [23,24]. In what follows, we focus on the force–time traces to unravel the characteristics of martensitic transformation.

Figure 3 (top row) depicts representative f–t traces acquired from independent and identical MD simulations in response to three different uniaxial displacement rates (left to right panels): $\dot{l}_x = 7.83 \times 10^{-4}$ Å/ps, 2.35×10^{-3} Å/ps,

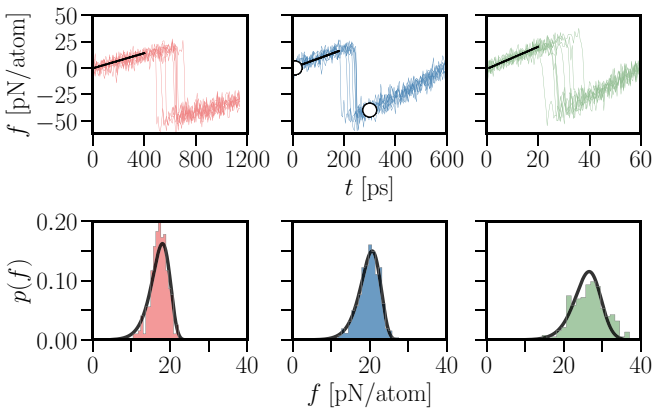

FIG. 3. Stochastic force-time responses. Top: Force, f, vs time sample traces from MD simulations for extension rates of 7.83×10^{-4} (left), 2.35×10^{-3} (middle), and 2.35×10^{-2} Å/ps (right). Black solid lines are $\langle f(t)\rangle$, and slopes $\partial_t \langle f(t)\rangle$ are the respective force rates $\dot{f} = 3.097 \times 10^{-2}$, 9.45×10^{-2}, and 0.9242 pN/ps per atom for the three cases. White circles mark the times of the snapshots in Fig. 1. Bottom: (Color bars) Probability density distribution of transition force, $p(f \mid \dot{f})$, corresponding to the peak forces seen in the top row. Black solid lines are the model predictions using Eq. (5).

and 2.35×10^{-2} Å/ps. An individual f–t trace increases linearly before reaching a certain level, f^*, which is referred to here as *transition* or *critical* force, just before falling sharply. Snapshots of local atomic configurations reveal that f^* corresponds to the onset of martensitic transformation [24]. The peak force has relaxed after stable martensite (product) has formed, relieving the stress in the deformed austenite lattice.

Force–time traces can be treated as signatures that reflect physical evolution of crystal lattice under mechanical deformation. Figure 1 (bottom row) depicts structural differences between initial unstressed austenite and post-transformed lattice after the transition is complete. Red and gray dots, which reference titanium and nickel atoms, respectively, are joined by a bond (line) if a pair of atoms has an interatomic distance less than or equal to 3 Å. Closely packed local directions clarify visualization of the lattice restructuring process during twinning, which involves an emergence of a *stacking fault* at the lattice scale and can be identified in the martensite structure. In Fig. 1 (bottom right), dashed vertical lines along $[001]_{B2}$—parallel to the z axis of B2 unit cell—indicate twin boundaries, delimiting a *stacking fault*. Symbols ↑ and ↓ denote directions of *shear*, driving atomic displacements off the native positions to produce an anomaly in the stacking sequence of atomic layers, causing the fault [22].

The instantaneous average force, $\langle f(t)\rangle$, grows linearly in time, t, associated with the regime of linear elasticity, prior to the occurrence of phase transition; see black lines, Fig. 3 (top row). So, a relation holds,

$$\langle f(t)\rangle = \dot{f}t \equiv f(t), \tag{1}$$

where $\dot{f} = \partial_t \langle f(t)\rangle$ translates into a constant rate of externally applied force prior to the transformation. We will use $\dot{f}$ in the place of $\dot{l}_x$ to denote an independent variable [25].

The f–t traces in Fig. 3 (top row) show that the critical force and the corresponding onset-time of transformation are statistically distributed. While a transition force observed in an individual trace is a random variable and cannot be predicted, a histogram of the set $\{f_1{}^*, f_2{}^*, \cdots, f_S{}^* | \dot{f}\}$ extracted from a large number ($S = 300$) of MD simulations at a given force-rate $\dot{f}$ is well defined; refer to Fig. 3 (bottom row). Further, the mean and standard deviation of the histograms (normalized) are found to trend positively with $\dot{f}$. It implies that as the force rate increases, a progressively higher force is needed to reshape austenite lattice because of prior lattice distortion. The implication is that the observed distribution, $p(f^*)$, which embodies microscopic fluctuations during phase transition, is an outcome of kinetic variability of the transformation mechanism, which we model in the next section.

B. Statistical mechanics of structural transitions

A microscopic process such as the activation of a crystallographic twin involving displacements of atomic planes is intrinsically probabilistic and can be modeled as a random walk. A description of a transition process as a random walk is provided by the Smoluschowski equation [15,16,26–29], which captures the evolution of a probability density function, $P(\xi, t \mid \xi = 0, t = 0)$, for observing the system state ξ at time t on a free-energy landscape $U(\xi, t)$; see Fig. 2. Here ξ is a variable denoting an order parameter of the system, and we consider $\xi \equiv \Delta l_x$ in the present case. When a quasistatic tensile force ramp is applied to the material, the equilibrium free-energy landscape is progressively deformed according to $U(\xi, t) = U_0(\xi) - f(t)\xi$, where $U_0(\xi)$ is the equilibrium (no force) free-energy profile [25]. $U_0(\xi)$ is assumed to consist of an attractor *well* domain with its local minimum in free-energy at the state $\xi = \xi_0 = 0$, and free-energy *barrier*, $\Delta U_\ddagger(f = 0) = U_0(\xi_\ddagger) - U_0(\xi_0) = U_\ddagger$ located at a *transition* state $\xi = \xi_\ddagger$. The well is mapped to the austenite (parent) phase, which is entrapped on one side of the barrier. To complete the transformation, the entrapped states are required to cross over the barrier to the other side—the martensite phase [30]. In general, landscape deformation is modeled in terms of the force-dependent landscape features, $\xi_0(f)$, $\xi_\ddagger(f)$, and $\Delta U_\ddagger(f) = U(\xi_\ddagger(f), f) - U(\xi_0(f), f)$, which accelerate the transformation dynamics in the presence of a tensile force.

The equation of motion of $P(\xi, t)$, captured in the Smoluschowski equation, is given as $\partial_t P(\xi, t) = -\partial_\xi J(\xi, t)$, where $J(\xi, t) = -(k_B T/\eta)\,\partial_\xi P(\xi, t) + (-\partial_\xi U(\xi, t)/\eta)\,P(\xi, t)$ is a probability flux of the escape of austenitic states by barrier crossing, and η is lattice friction constant of the restructuring of austenite in units of inverse time. A brief outline of the analytical solutions [15–17,26–29,31,32] is provided below. Under steady-state flux and an absorbing boundary located at the transition state, the differential equation can be expressed in terms of the survival probability of austenite phase, $\Psi(t) = \int_{-\infty}^{\xi_\ddagger} P(\xi, t)d\xi$, and further replacing the variable t by f using Eq. (1) gives

$$p(f) = -\frac{d\Psi(f)}{df} = \frac{\Gamma(f)\Psi(f)}{\dot{f}} \tag{2}$$

$$\Gamma(f) = \frac{k_B T}{\eta}\left[\int_{-\infty}^{\xi_\ddagger} d\xi \left\{ e^{-u(\xi,f)} \int_{\xi}^{\xi^+} d\xi_1 e^{u(\xi_1,f)} \right\}\right]^{-1}. \tag{3}$$

Here $p(f)$ is the transition force distribution; $\dot{f} = \partial_t \langle f(t) \rangle$ is the force rate; $u(\xi, f)$ is the free-energy in units of $k_B T$, i.e., $u(\xi, f) \equiv U(\xi, f)/(k_B T)$; and $\Gamma(f)$ is a reciprocal of mean passage time to escape the well and provides the force-dependent Kramers escape rate defining the austenite to martensite transition on a time-dependent free-energy landscape. The expressions of $p(f)$ and $\Gamma(f)$ facilitate the derivation of parameterized closed-form models for further analyses of force responses.

Parameterized expressions of $p(f)$ and $\Gamma(f)$ can be derived using an analytical free-energy function, $U_0(\xi) = U_\ddagger/2 + (3U_\ddagger/2\xi_\ddagger)(\xi - \xi_\ddagger/2) - (2U_\ddagger/(\xi_\ddagger)^3)(\xi - \xi_\ddagger/2)^3$, which has a form displayed in Fig. 2 [26,33]. Eq. (3) can be simplified if $(U_\ddagger/k_B T) \gg 1$ and a condition of quasistatic rate of change of the free-energy landscape, i.e., deformation applied on a timescale much longer in comparison to the timescale of phase transition, is assumed. These conditions permit the double integral to be expressed as a product of the inner and outer integrals, each evaluated in the subdomains of the well and barrier, respectively. Substitution of the free-energy function in Eq. (3) yields [26]

$$\Gamma(f) \approx \Gamma_0 \{1 - (f/f_c)\}^{1/2} e^{(U_\ddagger/k_B T)[1 - \{1 - (f/f_c)\}^{3/2}]}, \quad (4)$$

where $\Gamma_0 = \{1/(2\pi\eta)\} \cdot (6U_\ddagger/\xi_\ddagger{}^2)\, e^{-U_\ddagger/kT}$ is the rate constant at $f = 0$ and $f_c \equiv (3U_\ddagger/2\xi_\ddagger)$ is the maximal force to create martensite. Equation (4) shows that the rate of martensitic transformation can be increased exponentially by an applied force f. Even small values of force, $f \ll f_c$, can strongly accelerate the rate of crystallographic twinning according to $\Gamma(f) \propto \exp(f\xi_\ddagger/k_B T)$.

To derive an expression of the probability density distribution of transition force, $p(f)$; first, an expression of the survival probability function, $\Psi(f)$, is obtained by integrating Eq. (2), $\int_1^\Psi (\partial\Psi/\Psi) = -[\int_0^f \Gamma(f)\, \partial f]/\dot{f}$, after the substitution of $\Gamma(f)$ from Eq. (4). Second, employing the solution of $\Psi(f)$ in Eq. (2) (first equality) yields [29]

$$p(f \mid \dot{f}) = \frac{\Gamma(f) e^{\mu_0}}{\dot{f}} \exp\left\{-\mu(f)\left(1 - \frac{f}{f_c}\right)^{-1/2}\right\}, \quad (5)$$

where $\mu(f) \equiv (\Gamma(f)\, k_B T)/(\dot{f}\, \xi_\ddagger)$ and $\mu_0 \equiv \mu(f = 0)$. The expression, $p(f \mid \dot{f})\, df$, provides the conditional probability of the austenite to twinned martensite transition at an applied force f and loading rate $\dot{f}$. Equations (4) and (5) are the expressions that can be used to retrieve the intrinsic rate of transition (Γ_0), the activation free energy (viz., $U_\ddagger$), and the interaction range ($\xi_\ddagger$).

C. Energetic and kinetic properties of structural transitions

We evaluate the model outlined in the previous section to ascertain its predictive power through an analysis of an extensive set of force responses generated using MD simulations. Figure 4 shows the force spectra, where the symbols indicate simulation-derived force-dependent rates of phase transition, $\Gamma(f)$, at the three different strain rates. These were obtained by converting $p(f \mid \dot{f})$, which were extracted from the f–t traces and shown in Fig. 3 (bottom row, color shaded) using $\Gamma(f) = \dot{f}\, p(f \mid \dot{f})/\int_f^\infty df\, p(f \mid \dot{f})$ [29], a relation derived from Eq. (2). In addition, a *single* least-squares fit of Eq. (4)

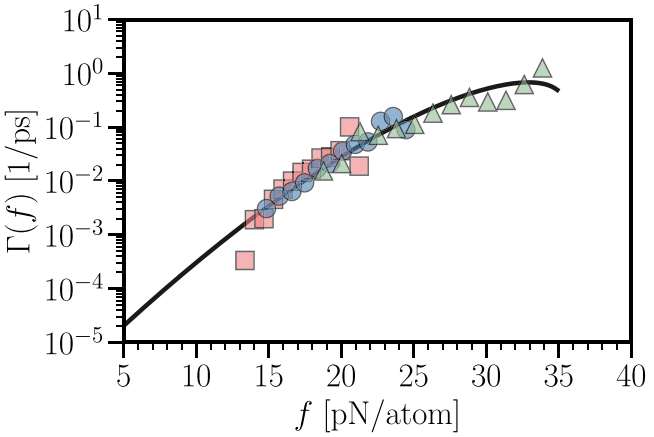

FIG. 4. Force dependent rate of martensitic transition—Force spectrum. Symbols are the values of $\Gamma(f; \dot{f}) \equiv p(f \mid \dot{f})/\int_f^\infty df\, p(f \mid \dot{f})$ obtained using the simulation data in Fig. 3 (bottom). The symbols □, ◯, △ correspond, respectively, to transition rates $\Gamma(f; \dot{f})$ where force rates are $\dot{f} = 3.097 \times 10^{-2}$, 9.452×10^{-2}, and 0.9242 pN/ps per atom, as in Fig. 3. A solid line is a fit of Eq. (4).

was performed on $\Gamma(f)$, choosing $k_B T = 41.4195$ pN Å, where $T = 300$ K is the temperature used in the simulations. The line of best fit is plotted in Fig. 4, and the best-fit parameter values obtained are $\Gamma_0 = 1.06 \times 10^{-6}$ 1/ps, $U_\ddagger = 620$ pN Å≈ 0.39 eV $\approx 15\ k_B T$, and $\xi_\ddagger = 26$ Å. The rate constant and the activation free energy obtained are found close to the estimates reported in Ref. [34]; however, in our case, the underlying rate process is due to the formation of pseudoelastic crystallographic twins and unrelated to a dislocation slip-based dynamics implicated in irreversible plastic deformation.

At the microscopic scale, the requirement of activation quantified in $U_\ddagger$ is primarily to promote nucleation and growth of stacking fault, which is at the core of twinned lattice development [22]. On average, $U_\ddagger$ translates to 0.39 eV/20 $\approx$ 20 meV activation free energy per unit cell distorted, given 20 unit cells along $[100]_{B2}$ (or x axis). Further, $\xi_\ddagger$ appears to correlate with the size of twin domain. This is confirmed in the simulation snapshot in Fig. 1(bottom right), which shows a spacing of $(\xi_\ddagger/a) = 26$ Å/3 Å ~ 9 unit cells between twin boundaries. The predictions, $p(f \mid \dot{f})$, after substitution of the extracted parameters in Eq. (5), are shown as solid lines in Fig. 3 (bottom row).

The agreement between analytical models, Eqs. (4) and (5), and simulation-derived observables over a large variation of applied strain rates substantiates the microscopic description based on statistical nonequilibrium framework of transition dynamics to provide a consistent interpretation of stochasticity observed in the isothermal force response patterns emerging from the process of martensitic phase transformation. Treatment of system-size and temperature-dependent force responses and the effects of undercooling on rate processes of nucleation [35], however, require further investigations. While we have relied on simulations to generate mechanical responses, we anticipate that the realization of probability distributions of critical forces is feasible using

nanomechanical techniques. By leveraging the theoretical approach described here, experimentally obtained distributions can be objectively interpreted for the recovery of microscopic properties—activation energy, interaction range (e.g., size of twin domain), and kinetic constant—defining the phase transformation.

III. CONCLUSIONS

Structural phase transformation in single crystalline metallic systems, triggered by controlled time-dependent deformation, reflects in the form of stochastic stress response patterns at the nanoscale. Such responses can be expressed in terms of statistical distributions. It is shown that a distribution function is interpretable and carries mechanistic information of the phase transition process. Mapping the phase transformation dynamics to a random probabilistic evolution of states over a time-dependent free-energy barrier is found to reliably elucidate the distribution of the critical phase-transition force and the force-dependent rate of transformation, providing an alternative route for accessing the otherwise hidden and innate mechanistic properties of a solid-to-solid transformation.

IV. METHODS

A. MD simulation

Nitinol, an alloy of titanium and nickel in equiatomic proportion, was simulated using classical MD [21]. The simulation box dimensions used were $l_x = 60$ Å, $l_y = 30$ Å, and $l_z = 30$ Å along the x, y, and z axes, aligned, respectively, to the [100], [010], and [001] crystallographic directions. Periodic boundary conditions were applied on every axis. The initial atomic configuration was created using *Atomsk* [36] by positioning 2000 atoms, each of titanium and nickel, on the lattice sites of a B2 supercell. The B2 unit cell structure (in essence, a body centered cubic lattice) had a lattice parameter of $a = 3$ Å before equilibration and the basis atoms were placed at (0, 0, 0) and (1/2, 1/2, 1/2) representing nickel and titanium, respectively, as shown in Fig. 1 (bottom left).

Equilibrium and nonequilibrium MD simulations were performed using LAMMPS [37,38]. The interatomic potential employed is the second-nearest-neighbor modified embedded-atom method developed by Ko *et al.* [39,40]. The positions and velocities of the atoms were evolved using a time step of 1 fs. The initial configuration was equilibrated for 1 ns under isothermal and isobaric conditions. Temperature and pressure were constrained using the Nóse-Hoover scheme at $T = 300$ K and $P = 1.013$ bar, respectively. The damping parameters used for the thermostat and barostat were 0.7 and 1 ps, respectively.

In the nonequilibrium MD simulations, the box was deformed at a fixed tensile strain rate along the x direction. To ensure that the initial configuration, the positions and velocities are distinct and random, an equilibration run of a duration of 1/2 ns preceded every simulation. The barostat was turned on only along the y and z directions, while the thermostat was active along all axes. The simulation box length, l_x, was ramped linearly in time according to $l_x(t) = \dot{l}_x\, t$ under the imposed rate of tensile displacement $\dot{l}_x$, which was kept constant. For statistical analyses, $S = 300$ simulations were performed for a given displacement rate. In all our simulations, a single twinned sublattice had formed.

The instantaneous resistive force generated per atom in the model system was computed as $f = \sigma_{xx} \cdot (A_{xx}/n)$, where σ_{xx} is a normal stress component of the internal stress tensor, (n/A_{xx}) is the number density of atoms in the yz plane (which has a normal along x axis) of the simulation box with $n = 100$, and $A_{xx} = l_z l_y$ is the cross-sectional area of the yz plane of the simulation box. The ensemble averages of the other elements of the stress tensor were approximately zero, showed no evidence of association with the phase transition signatures, and hence those elements were not considered in the analyses.

B. Data analyses

The raw data are comprised of force-rate ($\dot{f}$)-specific f–t traces; see Fig. 3 (top row). The time of occurrence of the peak (or transition) force, just prior to the sharp drop in force level, was extracted from every trace and enumerated for a given $\dot{f}$ as $\{\tau_1^*, \tau_2^*, \cdots, \tau_i^*, \cdots \tau_S^* \mid \dot{f}\}$, where i is an index of a simulation trace and $S = 300$ is the number of MD simulations performed per $\dot{f}$. The list of times is converted to $\{f_1^*, f_2^*, \cdots, f_i^*, \cdots f_S^* \mid \dot{f}\}$ via $f_i^* = \dot{f}\tau_i^*$ using Eq. (1) and transformed further into a *normalized* histogram of phase-transition forces, $p(f \mid \dot{f})$; see Fig. 3 (bottom row).

The force-dependent rate of martensitic transformation, shown as colored symbols in Fig. 4 for a given $\dot{f}$, is computed from the normalized histograms using $\Gamma_j(f_j \mid \dot{f}) = \dot{f}\, p(f_j \mid \dot{f}) / \sum_j^{n_b} f_j p(f_j \mid \dot{f})$, where Γ_j is the value of the transition rate at a force f_j corresponding to the jth bin of the histogram, and $n_b = 18$ is the number of bins in the histogram.

To recover the parameters $U_\ddagger$, $\xi_\ddagger$, and Γ_0 of martensitic transformation, Eq. (4) is fit to the data points $\{\cdots, (f_j, \Gamma_j), \cdots\}$ encompassing all three force-rates $\dot{f}$ used in this work. In the fitting procedure, a loss function $L(U_\ddagger, \Gamma_0, \xi_\ddagger)$, which is a sum of squared residuals,

$$L(U_\ddagger, \Gamma_0, \xi_\ddagger) = \sum_{\{\dot{f}\}} \sum_{j=1}^{n_b} [\ln \hat{\Gamma}_j(f_j \mid \dot{f}) - \ln(\Gamma_j)]^2, \qquad (6)$$

is minimized with respect to the variations of $U_\ddagger$, Γ_0, and $\xi_\ddagger$ using a *conjugate gradient* algorithm giving a reduced χ^2 value of 0.23 for the best-fit parameters. $\hat{\Gamma}_j$ is the predicted value of transition rate given by Eq. (4) at a force f_j. Note that Γ_j corresponding to the tail-regions ($|f - \mu_f| > 2\sigma_f$) of the normalized histograms $p(f)$, which had only a few samples, was excluded in the fitting process (μ_f and σ_f denote mean and standard deviation of a normalized histogram). Open-source Python libraries *pandas*, *matplotlib*, and *lmfit* were used for data analysis, charts, and nonlinear curve fitting.

[1] A. M. Minor and G. Dehm, MRS Bull. **44**, 438 (2019).
[2] R. Garcia, Chem. Soc. Rev. **49**, 5850 (2020).
[3] D. M. Dimiduk, M. D. Uchic, and T. A. Parthasarathy, Acta Mater. **53**, 4065 (2005).

[4] G. Dehm, B. N. Jaya, R. Raghavan, and C. Kirchlechner, Acta Mater. **142**, 248 (2018).

[5] W. F. Hosford, *Mechanical Behaviour of Materials* (Cambridge Univesity Press, 2010).

[6] K. Otsuka and X. Ren, Prog. Mater. Sci. **50**, 511 (2005).

[7] J. W. Christian and S. Mahajan, Prog. Mater. Sci. **39**, 1 (1995).

[8] I. J. Beyerlein, X. Zhang, and A. Misra, Annu. Rev. Mater. Res. **44**, 329 (2014).

[9] K. Bhattacharya and R. D. James, Science **307**, 53 (2005).

[10] J. M. McCracken, B. R. Donovan, and T. J. White, Adv. Mater. **32**, 1906564 (2020).

[11] G. B. Olson and M. Cohen, Metall. Trans. A **6**, 791 (1975).

[12] F. Falk, Acta Metall. **28**, 1773 (1980).

[13] M. Achenbach, Int. J. Plast. **5**, 371 (1989).

[14] Y. Chen, in *Handbook of Materials Modelling*, edited by W. Andreoni and S. Yip (Springer Nature, Switzerland, 2018), pp. 1265–1285.

[15] H. Risken, *The Fokker Planck Equation. Methods of Solution and Applications* (Springer-Verlag, Berlin, 1989).

[16] P. Hanggi, P. Talkner, and M. Borkovec, Rev. Mod. Phys. **62**, 251 (1990).

[17] L. B. Freund, Proc. Natl. Acad. Sci. USA **106**, 8818 (2009).

[18] J. S. Langer, Phys. Rev. Lett. **21**, 973 (1968).

[19] H. Kramers, Physica **7**, 284 (1940).

[20] See Supplemental Material at http://link.aps.org/supplemental/10.1103/PhysRevMaterials.6.043404 for predicted free-energy profiles and potential energy of the system computed from molecular dynamics simulations.

[21] D. Frenkel and B. Smit, *Understanding Molecular Simulation: From Algorithms to Applications*, Computational Science Series (Academic Press, San Diego, 2002), Vol. 1, 2nd ed.

[22] P. Chowdhury and H. Sehitoglu, Prog. Mater. Sci. **88**, 49 (2017).

[23] J. Ye, R. K. Mishra, A. R. Pelton, and A. M. Minor, Acta Mater. **58**, 490 (2010).

[24] J. A. Shaw and S. Kyriakides, Acta Mater. **45**, 683 (1997).

[25] A quasistatic protocol used in the simulations implies $\partial_\xi U(\xi, t) \approx 0$ for all t and ensures equality of the externally applied force, $f_a(t)$ and $\langle f(t)\rangle$.

[26] A. Garg, Phys. Rev. B **51**, 15592 (1995).

[27] E. Evans and K. Ritchie, Biophys. J. **76**, 2439 (1999).

[28] O. K. Dudko, a. E. Filippov, J. Klafter, and M. Urbakh, Proc. Natl. Acad. Sci. USA **100**, 11378 (2003).

[29] O. Dudko, G. Hummer, and A. Szabo, Phys. Rev. Lett. **96**, 108101 (2006).

[30] A second local minimum in free energy is expected corresponding to martensite for $\xi > \xi_\ddagger$ and has not been modelled.

[31] R. W. Friddle, Phys. Rev. Lett. **100**, 138302 (2008).

[32] A. Maitra and G. Arya, Phys. Rev. Lett. **104**, 108301 (2010).

[33] The linear-cubic polynomial is a third-order Taylor expansion of a continuous mathematical function about the inflection point, for instance, of a well-barrier energy function representing a single barrier transition process.

[34] K. Niitsu, H. Date, and R. Kainuma, Scr. Mater. **186**, 263 (2020).

[35] R. S. Aga, J. R. Morris, J. J. Hoyt, and M. Mendelev, Phys. Rev. Lett. **96**, 245701 (2006).

[36] P. Hirel, Comput. Phys. Commun. **197**, 212 (2015).

[37] S. Plimpton, J. Comput. Phys. **117**, 1 (1995).

[38] Y. Guo, X. Zeng, H. Chen, T. Han, H. Tian, and F. Wang, Adv. Mater. Sci. Eng. **2017**, 7427039 (2017).

[39] W. S. Ko, B. Grabowski, and J. Neugebauer, Phys. Rev. B **92**, 134107 (2015).

[40] L. Hale, Z. Trautt, and C. Becker, Interatomic potentials repository (2018), https://www.ctcms.nist.gov/potentials/, last accessed on 2021-04-30.